Computational Transonic Analysis of Canted Winglets

Bruce S Rosen*
Grumman Aerospace Corporation Bethpage New York

A computational method developed to provide a transonic analysis for upper/lower surface wing-tip mounted winglets is described Winglets with arbitrary planform, cant and toe angle and airfoil section can be modeled The embedded grid approach provides high flowfield resolution and the required geometric flexibility In particular coupled Cartesian/cylindrical grid systems are used to model the complex geometry presented by canted upper/lower surface winglets A new rotated difference scheme is introduced in order to maintain the stability of the small disturbance formulation in the presence of large spanwise velocities Wing and winglet viscous effects are modeled using a two dimensional strip boundary layer analysis. Correlations with wind tunnel and flight test data for three transport configurations are included

Nomenclature

A_1 A_2 A_3	= cylindrical grid scaling coefficients
a u v	= coefficients of transformed flow equation
B_1 B_2	= cylindrical grid scaling coefficients
b	= wingspan
C_1, C_2 C_3	= cylindrical grid scaling coefficients
C_p	= pressure coefficient
c	= section chord
c_{av}	= wing average chord
c_l	= section lift coefficient
g	= winglet geometry function
i j k	= mesh indices
M_∞	= freestream Mach number
s n	= characteristic coordinates
T U V	= nonlinear coefficients of flow equation
te	= trailing edge
u l	= upper lower
wlt	= winglet
x r θ	= cylindrical coordinates
x y z	= Cartesian coordinates
α	= angle of attack
γ	= specific heat ratio
Δx, Δr $\Delta\theta$	= cylindrical mesh spacing
η	= wing span position $= 2y/b$
φ	= perturbation velocity potential
ξ	= computational coordinate in x direction

Introduction

WING TIP mounted winglets are surfaces intended to provide reductions in wing drag at lifting conditions Whitcomb[1] noted that winglet design is still largely experimental in nature Theoretical methods have been limited to the calculation of optimum span load distributions for minimum induced drag[2,3] and to the subsonic analysis and optimization of winglets using lifting surface methods [4 5] These analyses are not capable of treating the nonlinear aspects of the transonic cruise condition flowfield Detrimental transonic effects can more than offset the lift induced drag benefits associated with winglets

Transonic methods have advanced to the point where these effects can be addressed The first practical technique for computing two dimensional inviscid transonic flows[6] has given rise to numerous three dimensional methods for the transonic analysis of wings and wing body combinations [7 13] The method developed by Boppe[14] can treat wing body combinations with various arrangements of pods nacelles pylons and a vertical upper surface winglet

These methods have used one of two basic approaches. The first and simpler, employs a modified small disturbance flow equation together with mean surface boundary conditions The second and more complex employs the full potential or Euler equation together with surface conforming boundary conditions Here, the problem of generating surface conforming grids can become more difficult than solving for the aerodynamic flowfield itself More exact methods are therefore not as advanced as small disturbance methods in their ability to treat complex shapes

The method described in this paper is an extension of Boppe's method[14] to include the treatment of upper/lower surface winglets with arbitrary planform cant and toe angle, and airfoil section A small-disturbance formulation is employed Embedded grid systems are used to attain a high degree of flowfield resolution to minimize computer resource requirements and to provide a large amount of geometric flexibility In particular, the complex geometry presented by canted upper/lower surface winglets has been modeled using coupled Cartesian/cylindrical grid systems Provisions have also been made for computing wing and winglet viscous effects

A new rotated difference scheme is introduced This scheme maintains the stability of the small-disturbance formulation in the presence of the large cross-flow velocities that can appear on winglets The scheme was originally developed for application to severely loaded, highly swept fighter wings It is expected that the scheme will prove useful for a variety of transonic flows characterized by large spanwise velocities

Correlations between computed winglet results and experimental data for three transport configurations are included These correlations illustrate the accuracy of the current method and indicate that it can be used to supplement the current iterative experimental approach to winglet design

Discussion

The present method employs a modified or extended transonic small disturbance flow equation The retention of additional terms found in the full potential equation makes it possible to resolve shock waves on wings with appreciable

Presented as Paper 84 0302 at the AIAA 22nd Aerospace Sciences Meeting Reno Nev Jan 9 12 1984; received Feb 6 1984; revision received June 25 1984 Copyright © American Institute of Aeronautics and Astronautics, Inc 1984 All rights reserved

*Engineer Aerodynamics Section. Member AIAA

sweep in the x y (wing) plane Written in terms of the disturbance velocity potential the global flow equation is[14]

$$\left[1-M_\infty^2-(\gamma+1)M_\infty^2\varphi_x-\frac{\gamma+1}{2}M_\infty^2\varphi_x^2\right]\varphi_{xx}$$
$$-2M_\infty^2\varphi_y\varphi_{xy}+[1-(\gamma-1)M_\infty^2\varphi_x]\varphi_{yy}+\varphi_{zz}=0 \qquad (1)$$

This equation is also used in the wing fine grid system

In the wing tip centered cylindrical grid, the wing and winglet surfaces lie in x-r planes To permit resolution of swept shock waves on these surfaces, the following flow equation is used in the cylindrical grid:

$$\left[1-M_\infty^2-(\gamma+1)M_\infty^2\varphi_x-\frac{\gamma+1}{2}M_\infty^2\varphi_x^2\right]\varphi_{xx}$$
$$-2M_\infty^2\varphi_r\varphi_{xr}+[1-(\gamma-1)M_\infty^2\varphi_x]\varphi_{rr}+\frac{1}{r}\varphi_r+\frac{1}{r^2}\varphi_{\theta\theta}=0 \qquad (2)$$

This is Eq (1) expressed in cylindrical coordinates with the x-y cross-flow terms represented by the equivalent x-r cross flow terms

Each winglet has a canted fine grid system in which the shock wave on the winglet may be swept in the canted x z (winglet) plane To improve the ability of the method to capture this type of shock wave, the following equation is used in the winglet fine grid systems:

$$\left[1-M_\infty^2-(\gamma+1)M_\infty^2\varphi_x-\frac{\gamma+1}{2}M_\infty^2\varphi_x^2\right]\varphi_{xx}$$
$$-2M_\infty^2\varphi_z\varphi_{xz}+[1-(\gamma-1)M_\infty^2\varphi_x]\varphi_{zz}+\varphi_{yy}=0 \qquad (3)$$

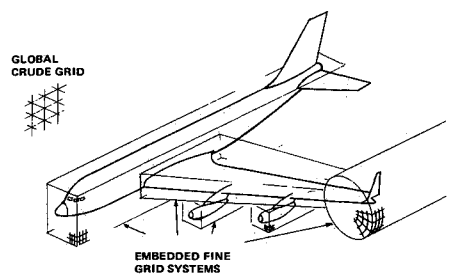

Fig 1 Multiple-grid approach for complex aircraft simulations

This is Eq (1) expressed in canted x-z coordinates with the x-y cross flow terms represented by the equivalent canted x z cross flow terms

Computational Grid Approach

The entire configuration is positioned in the center of a global Cartesian grid The global grid is stretched so that its boundaries represent infinity Flowfield resolution in high gradient regions is obtained by placing embedded grid systems about individual aircraft components Figure 1 illustrates a typical transport configuration with the aircraft component grid system boundaries included Communication between an embedded grid and the global grid (and, hence, other em bedded grids) takes place in an overlap region wherein the flow is computed twice This approach minimizes computing requirements while providing the geometric flexibility needed for treating complex realistic aircraft configurations

Canted upper and lower surface winglets present a geometrical arrangement that cannot be represented con veniently in the global Cartesian grid. To admit such geometry an embedded wing-tip centered cylindrical grid is employed Boundary conditions are easily imposed in the cylindrical grid, since all wing and winglet mean surfaces lie along coordinate lines

Canted winglet geometry does not need to be modeled explicity in the global grid A global grid inner boundary is defined in such a way that it completely encloses the wing-winglet computational region In this region no crude grid computations are performed An overlap region between the global grid inner boundary and the cylindrical grid outer boundary allows the two grid systems to interact Figure 2 illustrates the global grid/cylindrical grid boundary arrangement and the resulting overlap region

The cylindrical grid is evenly spaced in the radial (r) and angular (θ) directions Winglet cant angles are modified slightly so that winglet mean surfaces lie along the nearest angular cut (computed winglet results did not appear to be sensitive to small variations in cant angle). The cylindrical grid is split into three regions in the x- direction Grid stretch ing takes the same form as the global grid:

region I,

$$x=A_1+A_2\tan\left[\frac{\pi}{2}(\xi-\xi_1)\right]+A_3\tan\left[\frac{\pi}{2}(\xi-\xi_1)^3\right] \qquad (4a)$$

region II,

$$x=B_1+B_2\xi \qquad (4b)$$

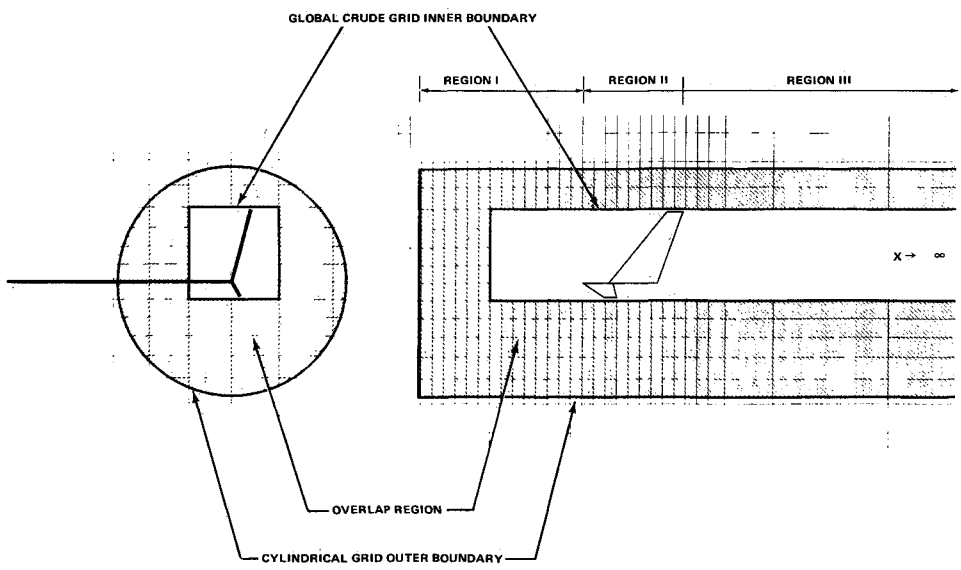

Fig 2 Global crude grid/cylindrical grid overlap region

region III

$$x = C_1 + C_2 \tan\left[\frac{\pi}{2}(\xi - \xi_2)\right] + C_3 \tan\left[\frac{\pi}{2}(\xi - \xi_2)^3\right] \quad (4c)$$

Region I is used to position the front of the cylindrical grid upstream of any high gradient regions The wing-tip and winglet surfaces are contained in region II, which is evenly spaced For computational purposes winglet position may be shifted axially by as much as 1 25% of the wing tip chord (a relatively small amount) Region III represents the winglet wakes that proceed to downstream infinity The stretching adds transform derivatives to the flow equation The following substitutions are made in Eq (2):

$$\varphi_x = \varphi_\xi \xi_x \quad (5a)$$

$$\varphi_{xx} = \varphi_{\xi\xi} \xi_x^2 + \varphi_\xi \xi_{xx} \quad (5b)$$

In order to improve flowfield resolution in high gradient regions close to the winglet surfaces, winglet fine grid systems are embedded within the cylindrical grid Each winglet has a separate fine grid system similar to that for the wing A two dimensional Cartesian array is set up at each position where a cylindrical grid r-station cuts the winglet surface The resulting fine grid system is skewed tapered, and canted to fit the winglet planform Figure 3 illustrates the final three level grid arrangement employed for simulating canted winglets

In addition to permitting canted winglet geometries the cylindrical grid also acts as an intermediate or medium density grid Without such a grid the great disparity in mesh size between the global crude grid and the relatively small winglet fine grid systems can result in a diverging solution

Finite Difference Approximations

For transonic flows characterized by large spanwise velocities, existing finite-difference schemes coupled with the modified small disturbance formulation can fail to produce stable solutions For example computations for severely loaded, highly swept fighter wings exhibited a wing tip stability problem due to significant cross flow velocities in that region A new rotated difference scheme was developed at Grumman that maintains the stability of such com putations Winglet calculations exhibited similar stability problems on the upper winglet inboard surface This problem was initially overcome by omitting cross flow terms (e g , $\varphi_r \varphi_{xr}$ and $\varphi_x \varphi_{rr}$) from the flow equations The new rotated difference scheme was then introduced The stability problem no longer appeared and cross flow terms are therefore retained in all of the flow equations used

Finite difference approximations are substituted for the derivatives in Eqs (1 3) The cylindrical grid flow equation will be used to illustrate the new rotated difference scheme The scheme is also employed for the winglet fine grid flow equation

Equation (2) can be written in the form

$$T\varphi_{xx} + U\varphi_{xr} + V\varphi_{rr} + (1/r)\varphi_r + (1/r^2)\varphi_{\theta\theta} = 0 \quad (6a)$$

where

$$T = 1 - M_\infty^2 - (\gamma+1) M_\infty^2 \varphi_x - \frac{\gamma+1}{2} M_\infty^2 \varphi_x^2 \quad (6b)$$

$$U = -2M_\infty^2 \varphi_r \quad (6c)$$

$$V = 1 - (\gamma - 1) M_\infty^2 \varphi_x \quad (6d)$$

Unlike the full potential equation, the characteristic directions of this equation are not symmetric with respect to the flow direction The present scheme is identical to Jameson's rotated difference scheme[15] except that the rotation is not into the direction of the flow Rather as shown in Fig 4b, the rotation is into the direction which bisects the characteristics of the flow equation For Eq (6a), this rotation occurs in the x r plane Denoting this direction as s (even though it is not the true streamwise direction), and that normal to it as n, Eq (6a) becomes

$$(a^2 - u^2 - v^2)\varphi_{ss} + a^2 \varphi_{nn} + (1/r)\varphi_r + (1/r^2)\varphi_{\theta\theta} = 0 \quad (7a)$$

where

$$u = \sqrt{\frac{-(T-V) + \sqrt{(T-V)^2 + U^2}}{2}} \quad (7b)$$

$$v = -\frac{U}{|U|}\sqrt{\frac{(T-V) + \sqrt{(T-V)^2 + U^2}}{2}} \quad (7c)$$

$$a = \sqrt{\frac{(T+V) + \sqrt{(T-V)^2 + U^2}}{2}} \quad (7d)$$

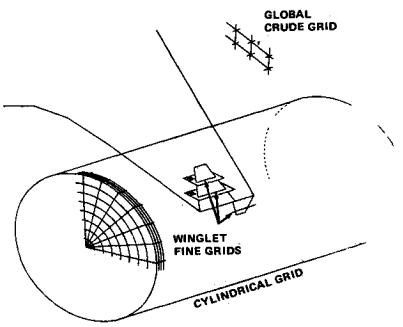

Fig 3 Three level grid arrangement for canted winglets

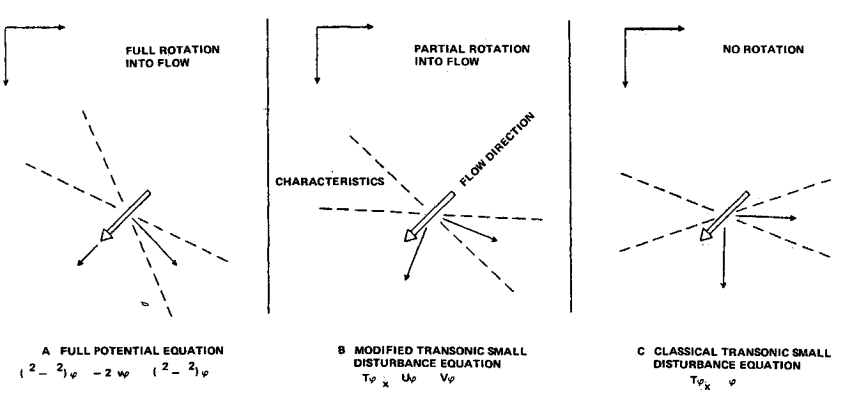

Fig 4 Rotated difference scheme

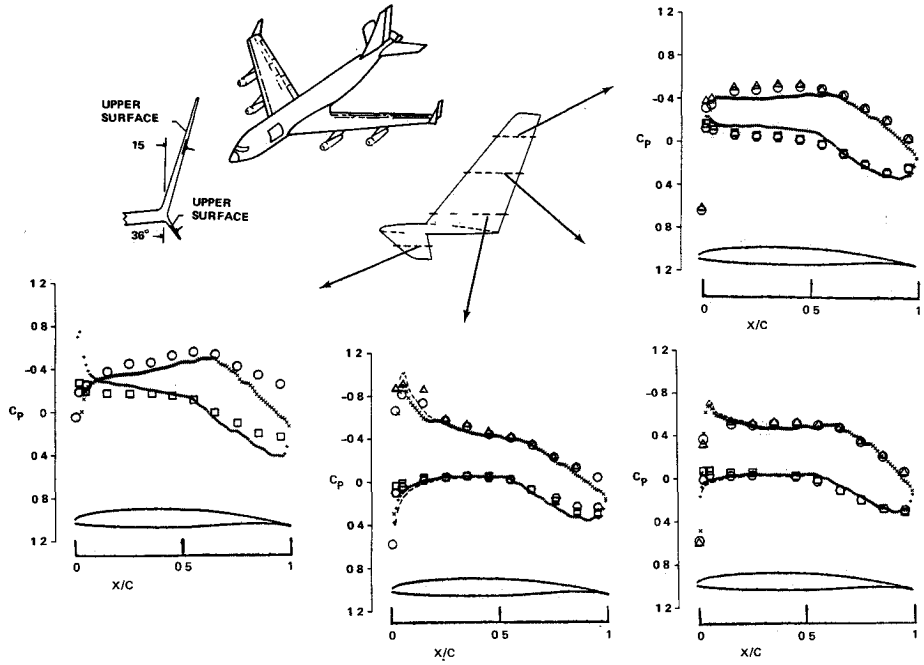

Fig 5 Boeing KC 135 canted winglet pressure distribution correlation; $M=0\ 78$ $\alpha=2\ 0$ deg lower winglet on/off

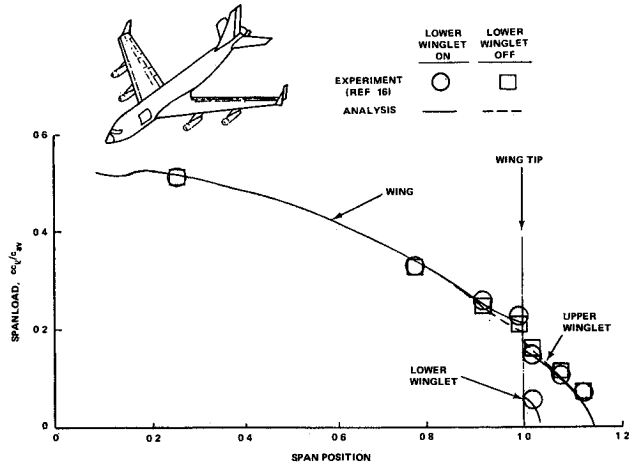

Fig 6 Boeing KC 135 canted winglet spanload correlation; $M=0\ 78$ $\alpha=2$ deg, lower winglet on/off

and

$$\varphi_{ss}=(u^2\varphi_{xx}+2uv\varphi_{xr}+v^2\varphi_{rr})/(u^2+v^2) \tag{7e}$$

$$\varphi_{nn}=(v^2\varphi_{xx}-2uv\varphi_{xr}+u^2\varphi_{rr})/(u^2+v^2) \tag{7f}$$

The present scheme is otherwise identical to that described in Ref 15 At subsonic points ($u^2+v^2<a^2$), central difference approximations are used for all terms contributing to φ_{ss} and φ_{nn} in Eqs (7e) and (7f) At supersonic points ($u^2+v^2>a^2$), upwind differences are used for terms contributing to φ_{ss} and central differences are used for those contributing to φ_{nn} All other derivatives occurring in Eq (7a) are centrally differenced Note that this new difference scheme reduces to the ones described in Refs 14 and 15, for the cases shown in Figs 4a and 4c, respectively

Wing and Winglet Surfaces

The winglets and their wakes are represented by planar surfaces of double valued grid points that extend from the winglet leading edges to downstream infinity For a winglet surface defined in canted y z coordinates by

$$y=g(x\ z) \tag{8}$$

the winglet tangency flow condition in the cylindrical grid is approximated by

$$(1/r)\varphi_\theta(x,r\ \theta_{\rm wlt})=g_x-\alpha\times\cos\theta_{\rm wlt} \tag{9}$$

or

$$\varphi_{k-1}\cong\varphi_{k+1}-2r\Delta\theta(g_x-\alpha\times\cos\theta_{\rm wlt}) \tag{10}$$

The boundary condition on the winglet upper surface becomes

$$\frac{1}{r^2}\varphi_{\theta\theta}=\frac{2\varphi_{k+1}-2\varphi_{k,u}-2r\Delta\theta(g_{x,u}-\alpha\times\cos\theta_{\rm wlt})}{(r\Delta\theta)^2} \tag{11a}$$

Similarly the winglet lower surface boundary condition becomes

$$\frac{1}{r^2}\varphi_{\theta\theta}=\frac{2\varphi_{k-1}-2\varphi_{k,l}+2r\Delta\theta(g_{x,l}-\alpha\times\cos\theta_{\rm wlt})}{(r\Delta\theta)^2} \tag{11b}$$

At the end of each sweep of the flowfield, the circulation at the winglet trailing edge is calculated:

$$\Gamma_{\rm wlt}=\varphi_u(x_{\rm te}\ r\ \theta_{\rm wlt})-\varphi_l(x_{\rm te}\ r\ \theta_{\rm wlt}) \tag{12}$$

The Kutta condition is enforced by requiring that the jump in potential across the winglet wake be equal to $\Gamma_{\rm wlt}$ For the wake upper surface, the jump condition is given by

$$\frac{1}{r^2}\varphi_{\theta\theta}=\frac{\varphi_{k+1}-2\varphi_{k,u}+(\varphi_{k-1}+\Gamma_{\rm wlt})}{(r\Delta\theta)^2} \tag{13a}$$

Similarly, the jump condition for the wake lower surface is given by

$$\frac{1}{r^2}\varphi_{\theta\theta}=\frac{(\varphi_{k+1}-\Gamma_{\rm wlt})-2\varphi_{k,l}+\varphi_{k-1}}{(r\Delta\theta)^2} \tag{13b}$$

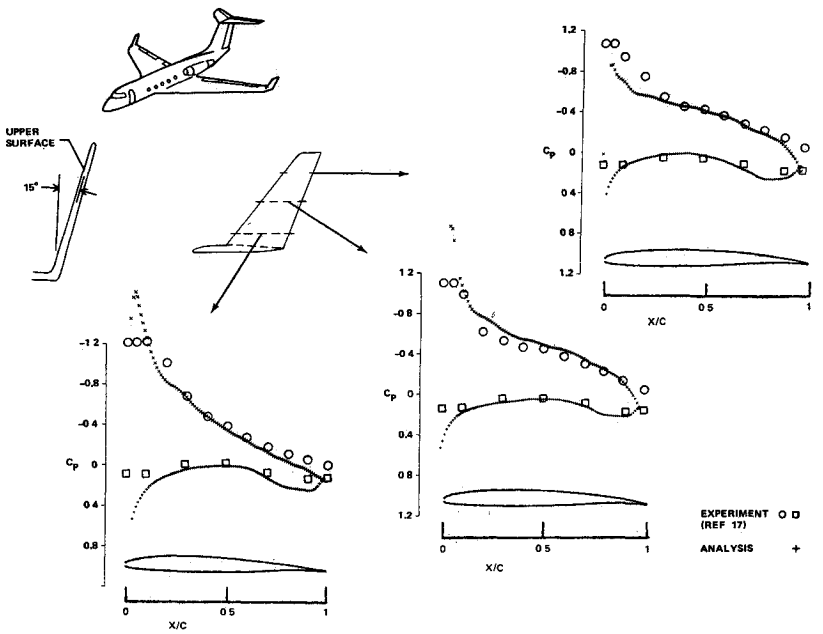

Fig 7 Gulfstream III canted winglet pressure distribution correlation; $M=0\ 75$, $\alpha=4\ 0$ deg

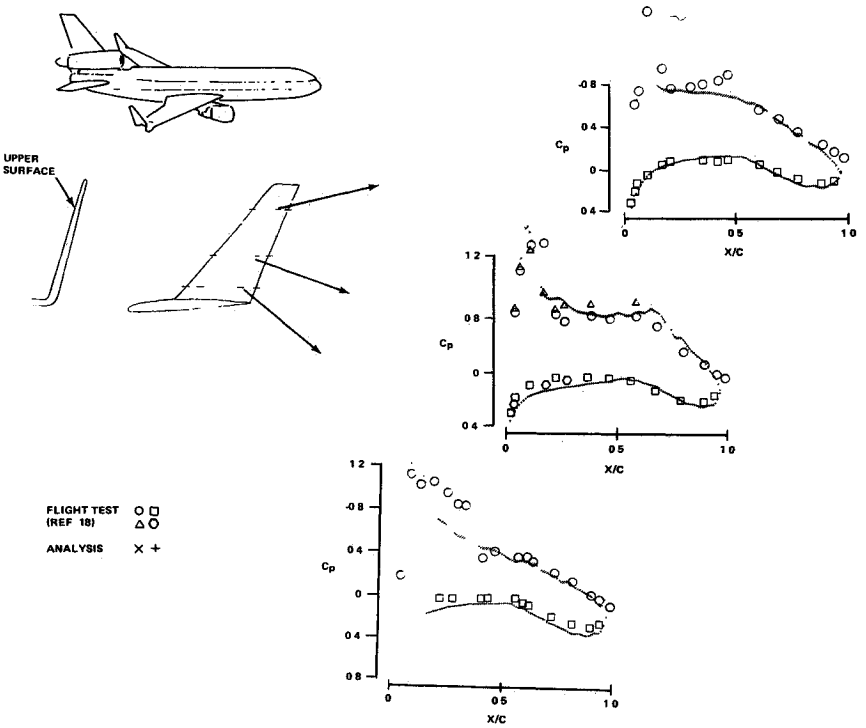

Fig 8 DC 10 ten foot winglet pressure correlation; $M=0\ 82$, $\alpha=3\ 2$ deg

Expressions similar to Eqs. (11) and (13) are used to impose boundary and jump conditions on the wing surface and the wing wake

Special care is required when imposing boundary con ditions in the wing-winglet or winglet winglet junction Often, the evaluation of a spanwise derivative on one surface in the usual manner would require differencing through the other surface When this situation occurs, a special first order accurate difference approximation is used to impose the adjoining surface's boundary condition

As a result of the small disturbance formulation employed, input winglet geometry should be modified to account for the rotation of the winglet planform with aircraft angle-of-attack For the cases presented in this paper, modified winglet leading edge sweeps and thickness distributions were used to simulate this effect

Wing and Winglet Viscous Effects

Wing and winglet viscous effects are computed in the present method by coupling a two dimensional "strip" boundary layer analysis with the aforementioned finite difference potential flow scheme. The modified Bradshaw turbulent boundary layer analysis described in Ref 14 is employed

When the full inviscid/viscous interaction is executed, wing and winglet fine grid pressure distributions are used for the boundary layer computations Surface boundary conditions are then modified to take into account the local slope of the boundary layer displacement thickness

Pressure Coefficients

Wing and winglet pressure coefficients are calculated from cylindrical grid potential values using the following formula:

$$C_p = -[2\varphi_x + (1-M_\infty^2)\varphi_x^2 + \varphi^2{}_r] \quad (14)$$

Winglet pressure coefficients are calculated from canted winglet fine grid system potential values using

$$C_p = -[2\varphi_x + (1-M_\infty^2)\varphi_x^2 + \psi_z^2] \quad (15)$$

Comparisons and Typical Results

Experimental data for the Boeing KC 135 configuration with upper/lower surface winglets can be found in Ref 16 In Fig 5 winglet pressure distributions computed using the present method are compared to data at the cruise condition $M=0\ 78$ and $\alpha=2$ deg Pressure distributions on both the upper and lower winglet show good correlation with the data Note that the downwash effect of the lower winglet on the upper winglet is predicted by the present method

Wing winglet spanloads for the above cases are shown in Fig 6 Theoretical and experimental spanloads agree well, as expected, based on the pressure distribution comparisons Note again the downwash effect of the lower winglet on the upper winglet

Experimental data for the Gulfstream III configuration with upper winglet can be found in Ref 17 Calculations were made using the present method for this configuration at the cruise condition $M=0\ 75$ and $\alpha=4$ deg Figure 7 shows that computed winglet pressure distributions compare well with the data for this case also

Experimental data for the Douglas DC 10 Series 10 configuration with winglets can be found in Refs 18 and 19 A 10-ft upper winglet and a reduced span 7 ft upper winglet were both flight tested Winglet pressure distributions were computed using the present method and a simulation of the DC 10 wing geometry. The results are compared with the data in Fig 8 for the 10 ft winglet (lower winglet-off) at the cruise condition Good correlation is indicated

For each of the above cases, the leading edge expansion level in the upper winglet root region is overpredicted, while pressures just aft of the expansion are underpredicted The reason for this discrepancy has not yet been determined

Concluding Remarks

A transonic computational method has been extended to include the treatment of canted upper/lower surface wing tip mounted winglets Wind tunnel and flight test data for three transport configurations were used to validate the new methodology Good correlation with data was shown for a variety of winglet geometries and flow conditions The new methodology represents an improvement over existing analyses because of its ability to treat the geometric complexity and nonlinear aspects (supercritical flow with shock waves) of winglet flowfields at transonic speeds It should prove useful for future winglet design efforts

Acknowledgments

This work was supported by NASA LRC under Contract NAS1 14732 The author would like to acknowledge C W Boppe of the Aerodynamics Section for providing assistance during development of the method and P Newman of NASA-LRC for suggesting the use of coupled Cartesian/cylindrical grid systems

References

[1] Whitcomb R T A Design Approach and Selected Wind Tunnel Results at High Subsonic Speeds for Wing Tip Mounted Winglets NASA TN D 8260 July 1976

[2] Weber, J Theoretical Load Distribution on a Wing With Vertical Plates, R&M No 2960 British A R C 1956

[3] Lundry J L., A Numerical Solution for the Minimum Induced Drag and the Corresponding Loading of Nonplanar Wings NASA CR 1218 Nov 1968

[4] Lamar J. E A Vortex Lattice Method for the Mean Camber Shapes of Trimmed Noncoplanar Planforms With Minimum Vortex Drag ' NASA TN D 8090, June 1976

[5] Goldhammer, M I 'A Lifting Surface Theory for the Analysis of Nonplanar Lifting Systems AIAA Paper 76 16 Jan 1976.

[6] Murman E M and Cole J D Calculation of Plane Steady Transonic Flows *AIAA Journal* Vol 9 Jan 1971 pp 114 121

[7] Bailey F R and Ballhaus W F Comparisons of Computed and Experimental Pressures for Transonic Flow About Isolated Wings and Wing Fuselage Configurations NASA SP 347 March 1975

[8] Albone C. M Hall M G and Joyce, G , Numerical Solutions for Transonic Flows Past Wing Body Combinations *Symposium Transsonicum II* Gottingen West Germany Sept. 1975 pp 541 548

[9] Schmidt W and Vanino R The Analysis of Arbitrary Wing Body Combinations in Transonic Flow Using a Relaxation Method ' *Symposium Transsonicum II* Gottingen West Germany Sept 1975 pp 523 532

[10] Klunker E B and Newman, P A Computation of Transonic Flow About Lifting Wing Cylinder Combinations, *Journal of Aircraft* Vol 11 April 1974, pp 254 256

[11] Caughey D A and Jameson A Numerical Calculation of Transonic Potential Flow About Wing Cylinder Combinations AIAA Paper 77 677 June 1977

[12] Caughey D A and Jameson A , Progress in the Application of Finite-Volume Methods to Wing Fuselage Calculations ' AIAA Paper 79 1513 July 1979

[13] Bailey F. R and Steger, J L , 'Relaxation Techniques for Three Dimensional Transonic Flow About Wings AIAA Paper 72 189, Jan 1972

[14] Boppe C W and Stern M A , Simulated Transonic Flows for Aircraft with Nacelles Pylons and Winglets AIAA Paper 80 0130 Jan 1980

[15] Jameson A Iterative Solution of Transonic Flow over Airfoils and Wings Including Flows at Mach 1 *Communications on Pure and Applied Mathematics*, Vol 27 May 1974 pp 283 309

[16] Montoya L C Effects of Winglets on a First Generation Jet Transport Wing NASA TN D 8474 July 1977.

[17] deKuyper, R E Wind Tunnel Tests of a 1/8 8 Scale Reflection Plane Model of the Grumman Gulfstream III Airplane ' Calspan Corporation Buffalo N.Y Report AA 4001 W-26 Nov 1977

[18] DC 10 Winglet Flight Evaluation Final Report Douglas Aircraft Company McDonnel Douglas Corporation Long Beach Calif Draft Report April 9 1982

[19] Gilkey R D Design and Wind Tunnel Test of Winglets on a DC 10 Wing NASA CR 3119 April 1979